Performance Analysis and Modeling Based on LTE-A Field Measurements: a City Center Example

Cetin Kurnaz (ckurnaz@omu.edu.tr)
Ondokuz Mayis University Faculty of Engineering: Ondokuz Mayis Universitesi Muhendislik Fakultesi
https://orcid.org/0000-0003-3436-899X
Ahmet Furkan Kola
Samsun University: Samsun Universitesi
Murat Oguz Esenalp
Turkcell

Research Article

Keywords: LTE-A, Field measurement, Throughput, CQI, TEMS Investigation

Posted Date: May 9th, 2022

DOI: https://doi.org/10.21203/rs.3.rs-1471579/v1

Performance Analysis and Modeling Based on LTE-A Field Measurements: a City Center Example

Cetin Kurnaz[1, *] Ahmet Furkan Kola[2], Murat Oguz Esenalp[3]

[1]Department of Electrical and Electronic Engineering, Ondokuz Mayıs University, Samsun, Turkey.

[2]Department of Electrical and Electronic Engineering, Samsun University, Samsun, Turkey.

[3]Turkcell Communications and Technology Company, Samsun, Turkey.

[*]Corresponding author, E-mail address: ckurnaz@omu.edu.tr, ORCID: 0000-0003-3436-899X

Abstract: The wireless communication channel is the critical parameter that affects the throughput in the LTE-A network. The user equipment measures the quality of the wireless channel as the channel quality indicator (CQI) value and transmits it to eNodeB. The eNodeB uses the CQI value to select the adaptive modulation and coding method to achieve the highest throughput. This study analyzes the LTE-A network based on actual field measurements. Measurements were taken at 80 different locations in Samsun (Turkey) city center using TEMS Investigation software. RSRP, RSRQ, SINR, CQI, and throughput values were recorded for each measurement in a stationary position while downloading 500 MB of data. Then, the averages of these recorded data were calculated, and detailed analyses were performed. At the end of the study, the effects of RSRP, RSRQ, SINR, and CQI on the throughput value in the LTE-A network were examined, and a novel mathematical model was proposed that gives the relationship between them with 88.85% accuracy. It has also been observed that the accuracy of the proposed model can be increased by 4% with GRNN. In the last stage of the study, a new CQI mapping method based on real-field measurements for the LTE-A system was developed.

Keywords: LTE-A, Field measurement, Throughput, CQI, TEMS Investigation.

1. INTRODUCTION

High data rate expectations of mobile users have been attempted to be met with the Release-8 LTE (Long Term Evolution) technology developed by 3GPP (3rd Generation Partnership Project) [1]. With Release-8, it is possible to achieve a bandwidth of up to 20 MHz on the downlink (DL) and data rates (throughput) of up to 100 Mbps with the multiple input multiple output orthogonal frequency division multiplexing (MIMO-OFDM) data transmission technique [2]. The LTE technology has been advanced with the 3GPP Release-10 LTE-Advanced (LTE-A) technology [3], and a new generation communication system can optimize itself and utilize frequency channels autonomously has begun. LTE-A technology continued to be developed with Release-11 [4], and Release-12 [5] was designed to meet users' higher data rate expectations with mobile applications and increase mobile traffic. The frequency band is used unordered using the non-contiguous intra-band scheme in Release-11, and spectral efficiency is enhanced. In Release-12, on the other hand, unordered usage coincides in various frequency bands with a non-contiguous inter-band system. By increasing the bandwidth with Release-12, high frequencies and high signal to interference plus noise ratio (SINR) values can be obtained for small cells. MIMO techniques can go up to 8x8, reduce system latency and intersymbol interference (ISI), increase channel quality, spectral efficiency, and throughput [6]. Release-12 can reach 750 Mbps downlink and 150 Mbps uplink (UL) throughput with a bandwidth of up to 100 MHz, MIMO-OFDM technology, and 256 QAM modulation.

LTE-A is a homogenous network that employs advanced base stations (eNodeBs, eNBs) to cover the whole cell and uses the same transmission power level, modulation technique, and antenna configurations to provide service to user units [7]. The downlink quality between eNodeB and user equipment (UE) in LTE-A systems is determined by wireless channel parameters. In the LTE-A system, the status of the wireless channel is expressed by the channel quality indicator (CQI). The CQI determined by the user unit is usually represented with the SINR

value calculated using reference signal received power (RSRP) and reference signal received quality (RSRQ). Depending on the user unit's CQI value sent to the eNodeB, the modulation scheme, transfer block size (TBS), and code rate of the data transmission are determined. Therefore, there is a direct relationship between CQI value and throughput (THRP). There are several pieces of research on the performance of LTE and LTE-A systems in the literature. Some of these are as follows; detailed practical performance analysis of the LTE cellular system based on field test measurements was evaluated [8], RSRP, RSRQ, and reference signal Signal to Noise Ratio at various points in space which is covered by an LTE macro base station operating at 2100MHz was measured [9], the effect of CQI, SINR, and other channel parameters on THRP was investigated in LTE and LTE-A networks [10-13]. The relationship of RSRQ and RSRP values with CQI, SNR, and their effect on THRP were investigated with actual field measurements [14-17]. Mathematical models have been proposed for the THRP calculation of system parameters in LTE networks [18, 19].

The LTE-A network field measurements were taken at 80 Samsun (Turkey) city center locations using the TEMS Investigation mobile network testing software. The RSRP, RSRQ, SIR, CQI, and THRP values were recorded for each measurement location. Detailed analyses were performed to investigate the relationships between RSRP, RSRQ, SINR, and CQI and evaluate their effects on THRP. As a result of the calculations, a new mathematical model has been proposed for the LTE-A system, which describes the relationship between the THRP value and the channel parameters.

The rest of the paper is organized as follows: Section II contains thorough information regarding LTE-A technology, Section III includes LTE-A field measuring technique. In Section IV, measurement results and analyzes are presented. Finally, the paper concluded in Section V.

2. LTE-A TECHNOLOGY

IMT-A standards determined by ITU-R were attempted to be met with LTE-A. The LTE-A system includes several advances, such as increased spectrum efficiency, carrier aggregation (CA), and the utilization of multiple antennas to deliver faster data rates than the LTE version. LTE-A makes better use of limited bandwidth by using more significant amounts of the radio frequency spectrum and innovative approaches. Users on an LTE-A network can use more than one band simultaneously and combine different bandwidths to increase the CA technique's efficiency. CA allows for higher data rates in LTE-A because it can provide a significantly broader transmission bandwidth by combining some component carriers (CC) in the same or separate frequency bands [20]. Thus, by combining the 1.4/3/5/10/15/20 MHz bandwidths (maximum five bands), 100 MHz bandwidth can be used. OFDM was first used as an access technique in the downlink in Release-8, and it was still used in Release-12. Carrier aggregation may be utilized efficiently using MIMO techniques that can be increased up to 8x8 in the downlink. A single user can use several frequency bands simultaneously. This method improves spectral efficiency and increases the user THRP value.

The main factors affecting data rate in an LTE-A network are the distance between transceivers if the line of sight (LOS), signal and noise power, bandwidth, and the number of users. The four essential radio resource management (RRM) metrics in the LTE-A network are; CQI, RSRP, RSRQ, and received signal strength indicator (RSSI) picked up by carrier. The wireless channel directly impacts system performance in the LTE-A

network, and all users estimate channel state information and transmit it to the eNodeB. CQI is crucial in LTE-A for the eNodeB to decide the corresponding modulation and encoding scheme. UE estimates CQI to maximize the data rate. CQI contains information regarding the wireless channel's quality, and each UE in the LTE-A network measures the SINR value, scales it to the CQI value, and reports this value to the eNodeB. The optimal modulation and coding method is selected by eNodeB for data transmission based on the current CQI value and starts data transmission to the user. 3GPP defines the RSRP, RSRQ, and RSSI measurements, whereas UE providers determine SINR. RSRP, RSRQ, and SINR have a critical role in CQI measurement.

The adaptive modulation and coding (AMC) system of the LTE-A network adjusts modulation techniques based on SINR and CQI values during communication, and the throughout varies correspondingly. AMC is a method for adapting to channel conditions that modify the modulation and coding scheme (MCS) based on the channel condition. SINR determines CQI, which defines the THRP that the UE can support under real-world radio conditions by adopting the modulation scheme. The higher the SINR for a measurement range, the higher the CQI and, thus, the THRP value. The maximum modulation scheme is 16-QAM, instead of CQI, which can take matters from 0-30 in Release-8. Along with LTE-A, in Release-10 and Release-11, the CQI takes values in 0-15, and the modulation scheme goes up to 64-QAM. While the CQI value range remained unchanged with Release-12, the maximum modulation technique was 256-QAM. THRP is therefore raised at high CQI levels. While there is no transmission when the CQI value is 0 with Release-12, QPSK modulation techniques are used between 1-4, 16-QAM between 5-7, 64-QAM between 8-12, 256-QAM modulation between 13-15. Table 1 shows CQI changes, modulation, SINR, and spectral efficiency for Release-12 [21]. As the table indicates, the CQI and spectral efficiency values improve as the SINR value increases.

Table 1. Changes in CQI, Modulation, SINR, and Spectral efficiency for Release-12

CQI	Modulation	SINR	Spectral efficiency
1	QPSK	-1.324	0.6016
2	QPSK	0.568	0.877
3	QPSK	2.460	1.1758
4	QPSK	4.352	1.4766
5	16 QAM	6.244	1.9141
6	16 QAM	8.136	2.4063
7	16 QAM	10.028	2.7305
8	64 QAM	11.920	3.3223
9	64 QAM	13.812	3.9023
10	64 QAM	15.704	4.5234
11	64 QAM	17.596	5.1152
12	64 QAM	19.488	5.5547
13	256 QAM	21.380	6.09375
14	256 QAM	23.272	6.863492
15	256 QAM	25.164	7.325397

The UE measures the RSRP and RSRQ parameters on the reference signal in the LTE-A network. RSRP and RSRQ are fundamental signal level and quality measures for LTE-A networks. RSRP and RSRQ are required to make a migration choice during intercellular movement. The RSRP is described as the linear average of the power contributions of the source components carrying the cell-specific reference signals throughout the

measurement frequency bandwidth. In other words, RSRP is the average power of resource elements (RE) carrying cell-specific reference signals (RS) across the entire bandwidth; therefore, RSRP is only measured on symbols bearing RS. In the LTE-A network, RSRP and RSRQ values indicate the quality of communication in dBm and dB, respectively. These variables are crucial in determining the frequency band in which the communication will occur. While the communication is in the mobile state, the RSRP and RSRQ decide which base station and cell to use for data transmission and handover [14]. On average, RSRP and SINR are proportional to each other.

The RSRP theoretically ranges from -140 dm to -44 dm in 1 dBm intervals and is reported as an integer value between 0 and 97 (The UE reports an integer value from 0 to 97, not the RSRP value). When the UE is as close to the eNodeB as possible, the signal quality is good, and the RSRP value is high; when the UE is further away, the signal quality is poor, and the RSRP value is low. RSRP levels for usable signals are typically about -70 dBm near the eNodeB and approximately -120 dBm at cell edges.

When RSRP is insufficient to find a solid intercellular migration or cell reselection choice, RSRQ measurement gives additional information. RSRQ is commonly used to obtain further details about channel quality and entire bandwidth. RSRQ may accept values ranging from -3 dB to 19.5 dB in 0.5 dB intervals, and the reporting range is an integer number ranging from 0 to 34. RSRQ is used to gather more information about channel quality and total bandwidth. Low RSRQ values (for example, -3 dB) indicate no interference, whereas high RSRQ values (for example, -19 dB) indicate a high level of interference.

Table 2 shows the evaluations of connection quality in the LTE-A network based on the RSRP, RSRQ, and SINR values [22]. Higher efficiency is obtained if the SINR is excellent for a measurement range; on average, RSRP and SINR are related, and the smaller the difference between RSSI and RSRP, the better the RSRQ.

Table 2. Signal level values versus signal quality

	Parameters	**RSRP (dBm)**	**RSRQ (dB)**	**SINR (dB)**
Signal Quality	Excellent	> -84	> -5	> 12.5
	Good	-85 to -102	-6 to -10	10 to 12.5
	Fair	-103 to -111	-6 to -10	7 to 10
	Poor	< -112	< -11	< 7

3. LTE-A FIELD MEASUREMENTS

In this study, TEMS software [23] was used to obtain field data at 80 different locations in Samsun city center to investigate the effect of CQI, SINR, RSRP, and RSRQ channel parameters on the THRP value in the LTE-A network. TEMS Investigation, an end-to-end network testing solution, allows testing features in a network to understand customer experience better and verify, optimize, and troubleshoot in a mobile network. Fig. 1 shows a visualization of the measurement sites. In Fig. 1, the gray lines represent the measurement route, and the stars represent the LTE-A base stations. The 17.2.5 version of the TEMS Investigation software and the Samsung Galaxy SM G920F as the EU were used. Fig. 2 shows a screenshot of the TEMS Investigation software captured during a measurement example. The Samsung Galaxy SM G920F terminal is classified as UE Cat6, ideally

supporting 300 Mbps DL throughput and 50 Mbps UL throughput [24]. The UE was held at about 1 m in the measurements. LTE-A Cat6 achieves high 4G speed with MIMO and CA (2x20 MHz). As multi-antenna technology, a 2x2 antenna structure is used. With LTE Cat 6, the highest throughout for the 20 MHz bandwidth is 150 Mbps. However, with CA, two bands of 20 MHz (40 MHz total) are combined to achieve a throughput of 300 Mbps.

Data were collected in 80 surrounded environments during the download process of 500 MB data. Because of the highest network demand throughout the working day, LTE-A measurements were taken during that time. Turkcell's mobile network was used to test LTE-A technology services. All measurements were made in an outdoor environment. At measuring locations, Turkcell LTE-A base stations use the LTE1800 (B3), LTE2100 (B1), and LTE2600 (B7) frequency bands.

Fig. 1. LTE-A field measurement route

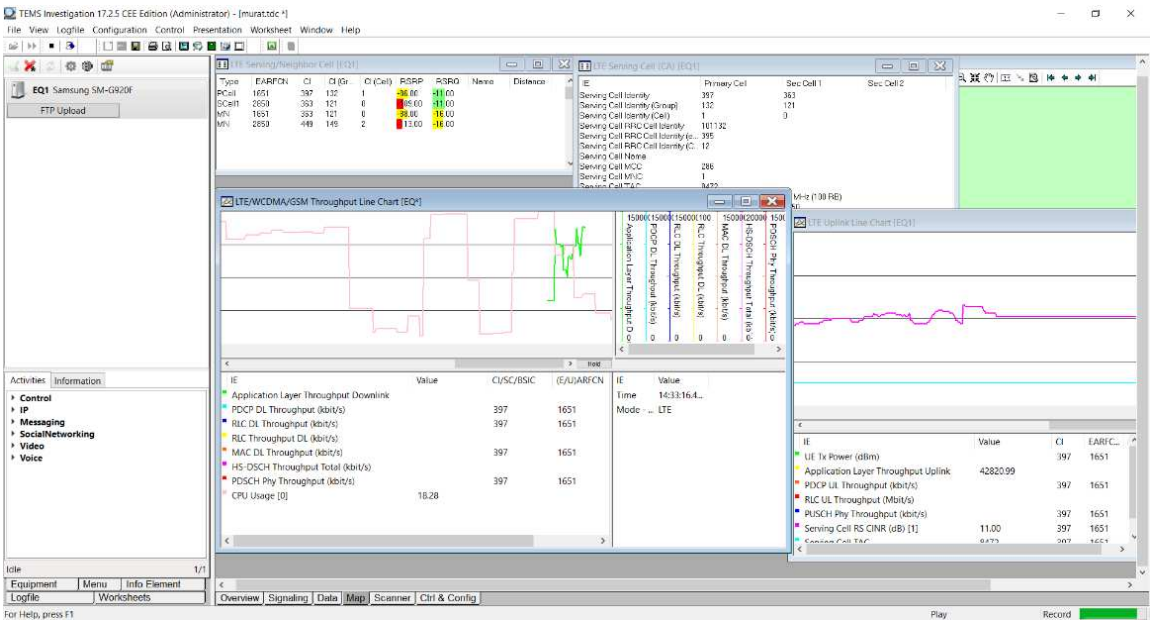

Fig. 2. A screenshot for the TEMS Investigation measurement

Regression Analysis

As a mathematical equation, regression analysis reveals the relationship between one or more independent variables and a dependent variable. In the simple linear regression model, the dependent variable Y and the independent variable X are defined as given below.

$$Y_i = \beta_0 + \beta_1 X_i + \epsilon_i \quad i = 1,2, \dots, n \tag{1}$$

Where β is the regression coefficient, n is the size of data and ϵ_i represents the error term.

The dependent variable is expressed with two or more independent variables (k).

$$Y_i = \beta_0 + \beta_1 X_{i1} + \beta_{12} X_{i2} + \cdots + \beta_k X_{ik} + \epsilon_i \quad i = 1,2, \dots, n \tag{2}$$

The matrix form of the multiple linear regression model is expressed as follows.

$$\begin{bmatrix} Y_1 \\ Y_2 \\ \vdots \\ Y_n \end{bmatrix} = \begin{bmatrix} 1 & X_{11} & \dots & X_{1k} \\ 1 & X_{21} & \dots & X_{2k} \\ \vdots & \vdots & \dots & \vdots \\ 1 & X_{n1} & \dots & X_{nk} \end{bmatrix} \begin{bmatrix} \beta_0 \\ \beta_1 \\ \vdots \\ \beta_k \end{bmatrix} + \begin{bmatrix} \epsilon_1 \\ \epsilon_2 \\ \vdots \\ \epsilon_n \end{bmatrix} \tag{3}$$

The most generic version of the multiple linear regression model is provided in equation (4).

$$Y = X\beta + \epsilon \tag{4}$$

Where Y is the nx1 dimensional vector of the actual data, X is the $nx(k+1)$ dimensional matrix of the input data, β represents the $nx1$ vector of the regression parameters, and ϵ is the error vector.

The vector B, which results in the lowest prediction error, is determined using the least-squares method with equation (5).

$$\hat{\beta} = (X^T X)^{-1} X^T Y \tag{5}$$

The normalized root mean squares error (NRMSE) approach may be used to test its accuracy between the anticipated and actual Y values. NRMSE value is calculated as given in equation (6).

$$\text{NRMSE} = \frac{\sqrt{\frac{1}{N}\sum_{n=1}^{N}(Y_n - \hat{Y}_n)^2}}{\max(Y) - \min(Y)} \tag{6}$$

Where Y_n is the real, $\hat{Y}_n$ is the predicted value, n is the index number, and N represents the total number of data.

Generalized Regression Neural Network:

Generalized regression neural network (GRNN) was first proposed by Specht to overcome the disadvantages of feed-forward backpropagation (FFBP) networks [25]. The GRNN model is a kernel regression network-based variation of radial basis neural networks [26]. GRNN has fast computational speed and good nonlinear approximation performance [27, 28]. GRNN does not require an iterative training approach such as backpropagation to identify model parameters. It approximates any function between input and output values and derives the function prediction directly from the training data. In GRNN, the prediction error approaches zero as the size of the training data increases. The sigmoid activation function, commonly used in ANN, is replaced with a radial basis function (RBF) in GRNN. The probability density function is estimated using Parzen's non-

parametric estimator [29]. The smoothing factor (σ) is the only variable in GRNN that represents the width of the RBF. Unlike traditional ANN networks, which have three layers, as shown in Fig. 3, GRNN has a four-layer network structure [30, 31] that includes input, pattern, summation, and output layers. The pattern layer consists of radial basis functions, and the summation layer consists of linear functions. A radial basis function is a Gaussian function with a bias of a smoothing factor in the pattern layer. Training dataset, $[x_1, x_2, \ldots, x_n]$ consists of input values, and there is an output value corresponding to each input $[y_1, y_2, \ldots, y_k]$.

The input layer is used to input parameters which are then passed to the pattern layer. The output of the i^{th} pattern node is expressed as P_i and is calculated as given below.

$$P_i = \exp\left[-\frac{(x-x_i)^T(x-x_i)}{2\sigma^2}\right], i = 1,2,\ldots,m \tag{7}$$

Where x variables are inputs, x_i is the learning sample for the ith neuron, and σ is the standard deviation of the input parameter, which is also known as the smoothing factor.

The summation layer consists of two types of summation methods, as shown by equations (8) and (9). One performs an arithmetic summation of the output of all neurons in the pattern layer. In contrast, the other neuron performs a weighted summation of the output of all neurons in the pattern layer.

$$S_d = \sum_{i=1}^{m} P_i, \quad i = 1,2,,\ldots,m \tag{8}$$

$$S_k = \sum_{i=1}^{m} w_{ij} P_i, \quad j = 1,2,,\ldots,k \tag{9}$$

Where w_{ij} is the weight value of the i^{th} neuron in the pattern layer to summation layer, and the j^{th} neuron is the j^{th} element of the output layer.

The value of neural node k in the output layer can be expressed with y_k as:

$$y_k = \frac{S_k}{S_d}, k = 1,2,,\ldots,n \tag{10}$$

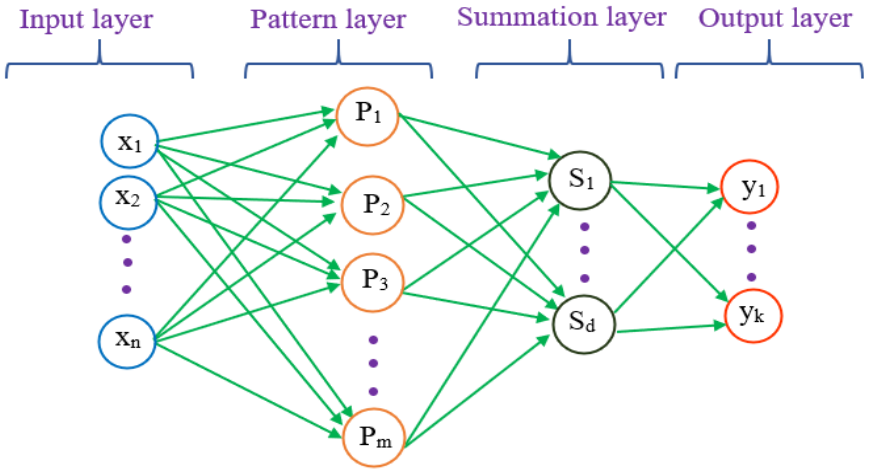

Fig. 3. The structure of GRNN

4. MEASUREMENT RESULTS AND ANALYSIS

Fig. 4 shows the LTE-A network measurement results for measurement location 1 (L1). The data were collected during downloading processes of 500 MB data files at L1. 500 MB of data was downloaded in 65.8 sec, the highest throughput was 81.39 Mbps, and the average throughput was 60.86 Mbps for L1. Fig. 4 shows the RSRP, RSRQ, SINR, CQI, and THRP changes recorded during 65.8 sec. As can be seen in the figure, these five measurement parameters can also change depending on the intensity of use of the system, even in the stationary measurement position. Table 3 shows statistical evaluations for RSRP, RSRQ, SINR, CQI, and THRP recorded during the 65.8 sec measurement period. Since the mean values were taken into account in the system evaluations in the [32, 33] studies, the evaluations were made on the average values in this study.

Table 3. Statistical evaluations for L1

	Max.	Min.	Mean	STD
RSRP (dBm)	-89.89	-94.14	-92.04	0.80
RSRQ (dB)	-7.80	-14.90	-11.80	1.60
SINR (dB)	16.34	6.39	11.36	2.20
CQI	11.30	7.50	9.62	0.89
THRP (Mbps)	81.39	41.68	60.86	12.32

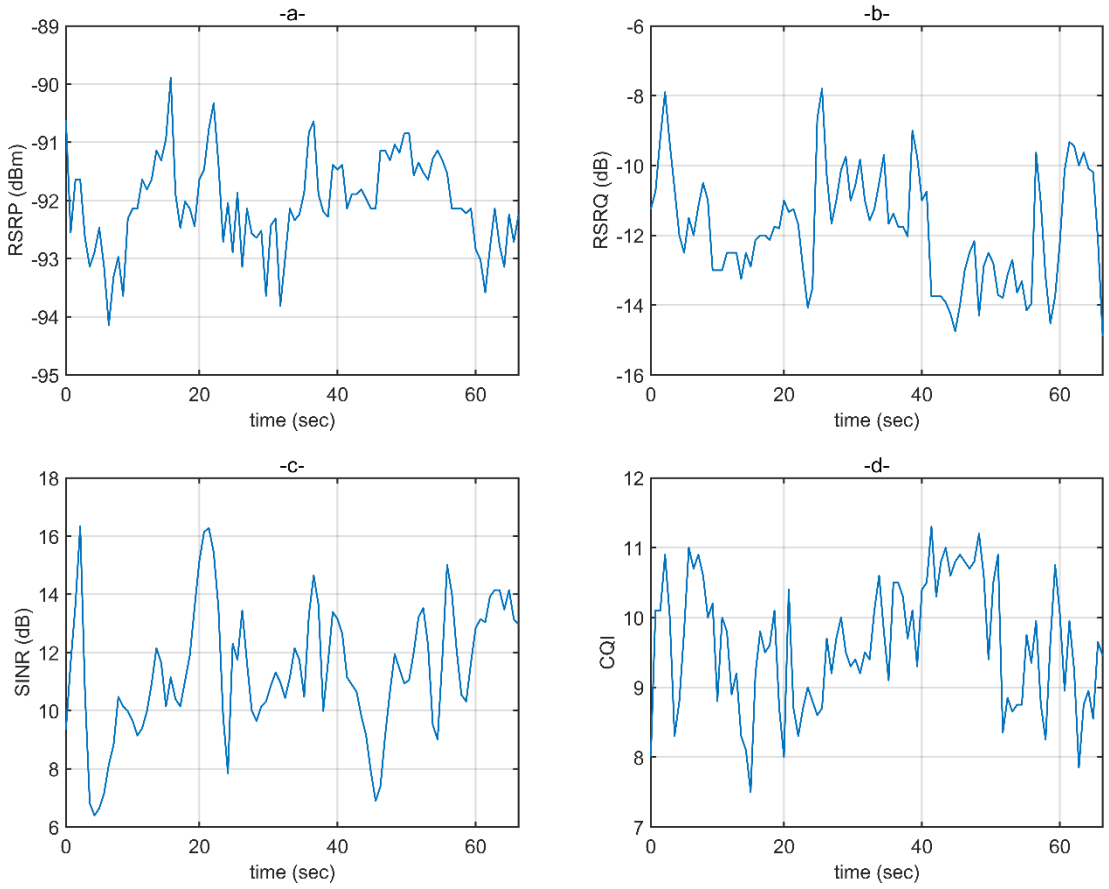

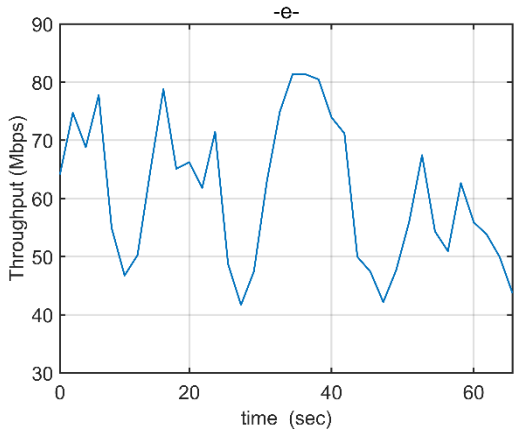

Fig. 4. a) RSRP, b) RSRQ, c) SINR, d) COI, and e) THRP values for L1

All analyses in this study were performed by taking the average of the RSRP, RSRQ, SINR, CQI, and THRP values recorded during the download of 500 MB of data for 80 locations. Fig. 5 illustrates box graphs of mean RSRP, RSRQ, SINR, CQI, and THRP values. In the figure, the blue box shows the boundaries of the data, and the red line shows the median value, the green diamond shows the mean value. When considering Fig.5, the RSRP value varies from -118.98 dBm to -77.37 dBm, with an average of -93.43 dBm and a median of -91.86 dBm. The RSRQ ranges from -12.11 dB to -6.95 dB, with an average value of -9.27 dB and a median value of -9.18 dB. The SINR ranges from 6.46 dB to 23.41 dB, with an average of 14.31 dB and a median of 14.42 dB. The CQI ranges from 9.27 to 13.58, with an average of 11.43 and a median of 11.56. THRP ranges from 34.80 Mbps to 102.10 Mbps, with an average of 68.83 Mbps and a median of 65.78 Mbps.

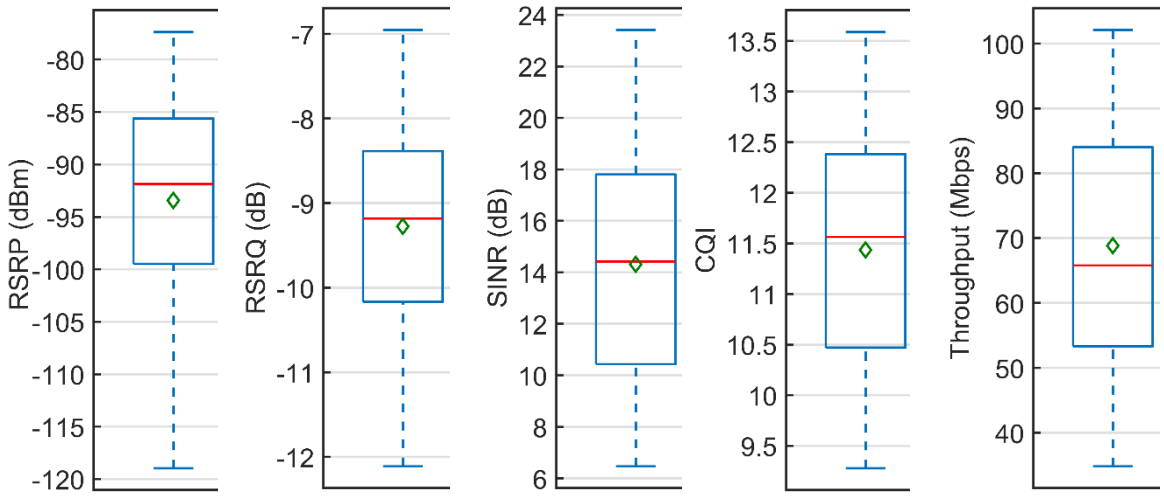

Fig. 5. Box graphs for LTE-A network measurements RSRP, RSRQ, SINR, CQI, and THRP data

Fig. 6 shows cumulative distribution function (CDF) graphs of mean RSRP, RSRQ, SINR, CQI, and THRP values. Considering the signal levels shown in Fig.6 and Table 2, 18.52 percent is more significant than -84 dBm, and the signal quality is excellent for RSRP. Only 5.32% of the measurements are below -112 dBm. The RSRQ has no values more than -5dB, 91.05% of measures are above -11dB and just 16.9% are weak. SINR data is 65.7 percent over 12.5 dB, and just 5.5 percent is below 7dB.

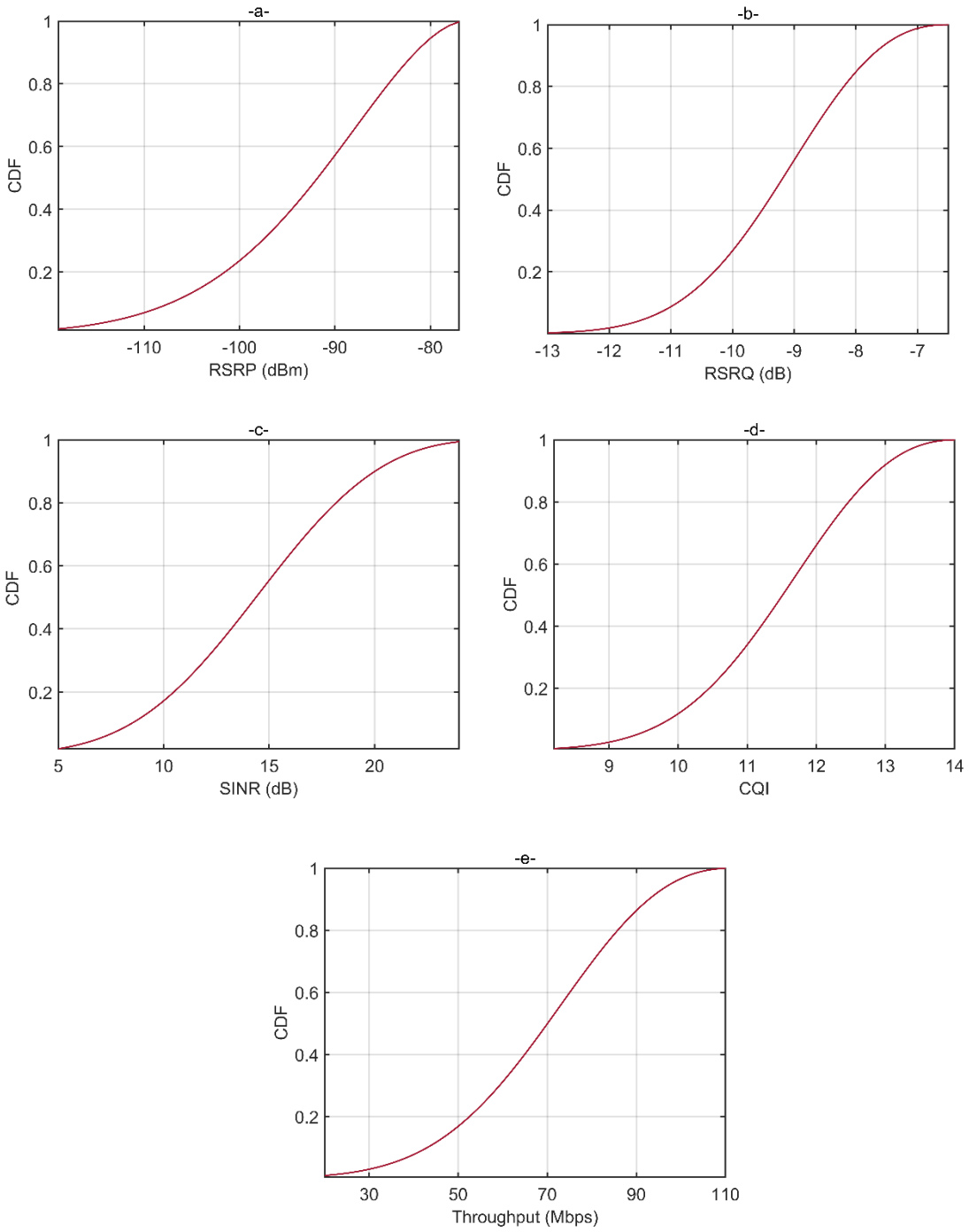

Fig. 6. CDF values for a) RSRP, b) RSRQ, c) SINR, d) COI, and e) THRP

The correlation coefficients (CC) between RSRP, RSRQ, SINR, CQI, and THRP were also analyzed and are shown in Table 4. When the table is analyzed, the highest correlation is found between 0.8418 and CQI and THRP. The second highest correlation is between SINR and CQI with 0.8393.

Table 4. Correlation coefficients between RSRP, RSRQ, SINR, CQI, and THRP

CC	RSRP	RSPQ	SINR	CQI	THRP
RSRP	1	0.6512	0.6130	0.6175	0.7785
RSRQ	0.6512	1	0.6490	0.6681	0.7355
SINR	0.6130	0.6490	1	0.8393	0.8134
CQI	0.6175	0.6681	0.8393	1	**0.8418**
THRP	0.7785	0.7355	0.8134	**0.8418**	1

Fig. 7 depicts the relationship between THRP and RSRP, RSRQ, SINR, and CQI statistics. Fig. 7 shows that when the RSRP, RSRQ, SINR, and CQI values increase, so do the THRP values.

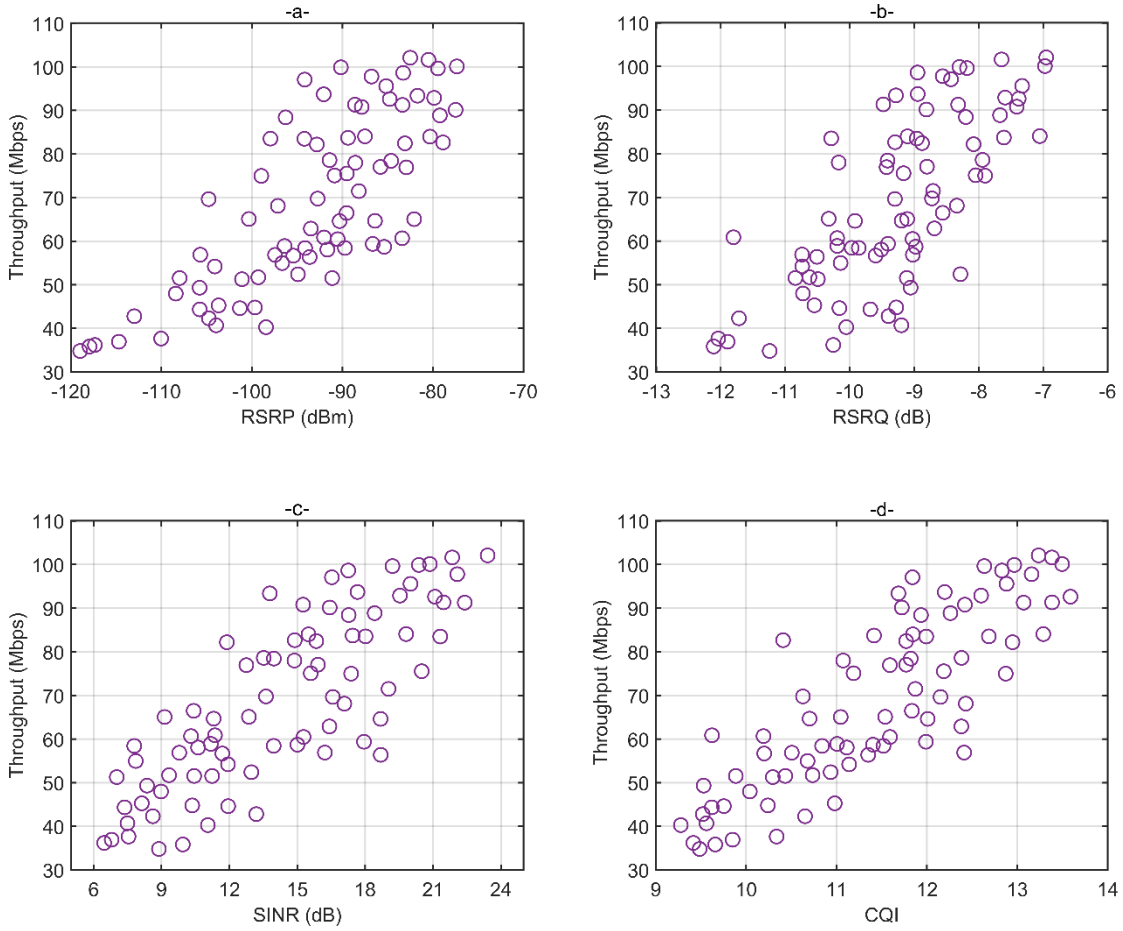

Fig. 7. Mean user throughput versus a) RSRP, b) RSRQ, SINR, d) CQI

Regression analyses were performed on the data to determine the mathematical formulation of the link between THRP and RSRP, RSRQ, SINR, and CQI. For clarity, RSRP X_1, RSRQ X_2, SINR X_3, CQI X_4, and THRP are denoted as Y. The relationship between X_1 and Y can be expressed using simple regression analysis, as seen in equation (11).

$$\hat{Y} = 209.9914 + 1.5108X_1 \tag{11}$$

Using equation (6), the NRMSE error between the predicted Y ($\hat{Y}$) using X_1, and the real Y was estimated to be 0.1819.

Equations (12), (13), and (14) yield calculated Y values using X_2, X_3 ve X_4.

$$\hat{Y} = 178.5832 + 11.8343X_2 \quad (12)$$

$$\hat{Y} = 18.7250 + 3.5010X_3 \quad (13)$$

$$\hat{Y} = -90.9329 + 13.9706X_4 \quad (14)$$

While the NRMSE error between the estimated Y using equation (12) and the real Y value is 0.1964, the NRMSE errors for equations (13) and (14) are 0.1686 and 0.1565, respectively.

Multiple linear regression analysis was used to estimate the Y value using X_1, X_2, X_3, and X_4 to improve estimation accuracy and reduce the NRMSE value. The mathematical expression obtained from multiple regression analysis is given in equation (15).

$$\hat{Y} = 66.7375 + 0.6469X_1 + 2.1683X_2 + 0.9240X_3 + 6.0699X_4 \quad (15)$$

The NRMSE error between the estimated Y and the measured Y value using equation (15) is 0.1155. Utilizing four-channel variables and multiple regression analysis improves prediction accuracy by around 2.5%. Fig. 8 shows the variation in measured and estimated THRP levels based on measurement location.

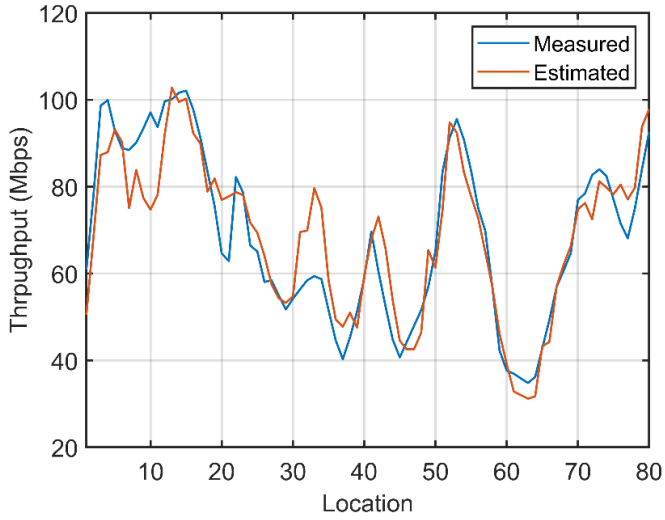

Fig. 8. Variation in measured and estimated THRP based on measurement location

To find the better relationship (i.e., lower NRMSE) between THRP and RSRP, RSRQ, SINR, and CQI, the GRNN method was applied to data using MATLAB software (MATLAB® 2020b). In simulations, 70% of the data were randomly used for training (56), and 30% were used for testing (24). This process was repeated 1000 times, and the minimum NRMSE was selected. Table 5 lists the parameters used in the simulation. In this study, only the result of the 0.85 value of spread of radial basis function is given because it gives the lowest NRMSE in simulations. As a result of the simulation, the lowest NRMSE value was calculated as 0.0191 for training and 0.0714 for testing. The regression performances of the GRNN method for training, testing, and all data are shown in Fig. 9 a–c, respectively.

Table 5. Parameters of the GRNN method

Parameters	NRMSE	
Inputs: 4, (X_1, X_2, X_3, X_4)	Training	Testing
Outputs: 1, (Y) **Spread of radial basis functions:** 0.85 **MATLAB functions:** newgrnn	0.0191	0.0714

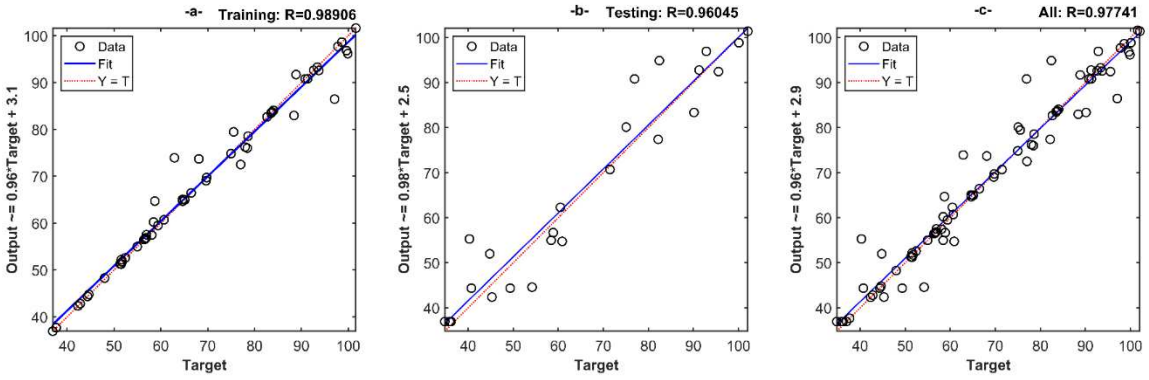

Fig. 9. Regression graph for a) training, b) testing, and c) all data

In the last stage of the research, in addition to the THRP analyses in the LTE-A network, the relationship between SINR and CQI was examined. The relationship between SINR and CQI is defined in the literature as given in equation (16) [21]. Using equation (16), the NRMSE value between the estimated THRP and the measured THRP is 0.6184. Therefore, the methodologies described in the literature are insufficient to express real-world measurements. For this reason, the relationship between SINR and CQI was obtained as given in equation (17) by applying linear regression analysis to the measurement data.

$$\widehat{X}_4 = 1.7 + 0.5285X_3 \tag{16}$$

$$\widehat{X}_4 = 8.3205 + 0.2177X_3 \tag{17}$$

The NRMSE between the estimated and measured CQI values using equation (17) is 0.1482. Fig. 10 shows the SINR CQI graph for the measured, theoretical, and proposed techniques. The figure shows that the SINR-CQI matching method used in the literature is much below the actual LTE-A network data.

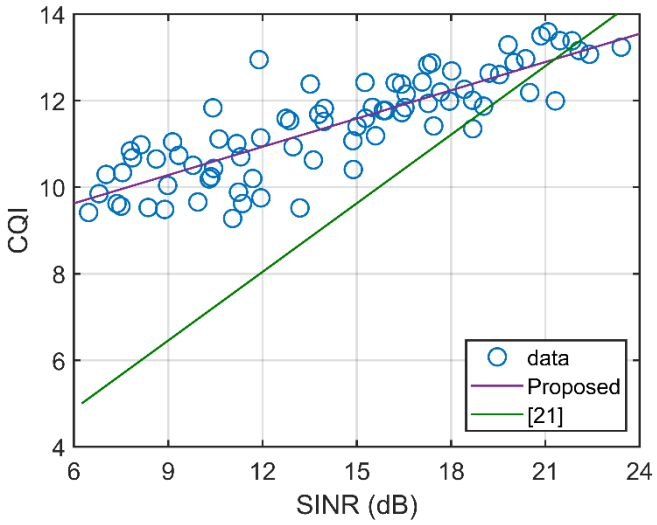

Fig. 10. SINR CQI mapping method

5. CONCLUSION

In this study, real-time throughput analyses were made for the LTE-A network. LTE-A network measurements were taken at 80 distinct points in Samsun's city center for this purpose. For each measurement 500-MB file is uploaded to Dropbox, and RSRP, RSRQ, SINR, CQI ve THRP values are recorded. The relationship between THRP and RSRP, RSRQ, SINR, and CQI was analyzed and modeled mathematically. The accuracy of the mathematical model between RSRP and THRP is 81.8%, while the accuracy for RSRQ, SINR, and CQI is 80.3%, 83.1%, and 84.3%, respectively. The THRP model using RSRP, RSRQ, SINR, and CQI has an accuracy of 88.85%. To increase the model accuracy, the GRNN structure was used, and THRP was estimated with an accuracy of up to 92.86%.

REFERENCES

[1] 3GPP, "3rd Generation Partnership Project; Technical Specification, LTE; Evolved universal terrestrial radio Access (E-UTRA); Long Term Evolution (LTE) physical layer; General description, 3GPP TS 36.201 version 8.3.0 Release 8.

[2] Toskala, A., Holma, H., Pajukoski, K., & Tiirola, E. (2006, September). UTRAN long term evolution in 3GPP. In 2006 IEEE 17th International Symposium on Personal, Indoor and Mobile Radio Communications (pp. 1-5). IEEE.

[3] 3GPP, "3rd Generation Partnership Project; Technical Specification, LTE; Evolved universal terrestrial radio Access (E-UTRA); Long Term Evolution (LTE) physical layer; General description, 3GPP TS 36.201 version 10.0.0 Release 10

[4] 3GPP, "3rd Generation Partnership Project; Technical Specification, LTE; Evolved Universal Terrestrial Radio Access (E-UTRA); User Equipment (UE) radio access capabilities (3GPP TS 36.306 version 11.4.0 Release 11)

[5] 3GPP, "3rd Generation Partnership Project; Technical Specification, LTE; Evolved Universal Terrestrial Radio Access (E-UTRA); User Equipment (UE) radio transmission and reception (3GPP TS 36.101 version 12.5.0 Release 12)

[6] Everett, E., Shepard, C., Zhong, L., & Sabharwal, A. (2016). SoftNull: Many-antenna full-duplex wireless via digital beamforming. *IEEE Transactions on Wireless Communications*, *15*(12), 8077-8092.

[7] Khan, S. A., Asshad, M., Küçük, K., & Kavak, A. (2018). A power control algorithm (PCA) and software tool for femtocells in LTE-A networks. *Sakarya University Journal of Science*, *22*(4), 1124-1129.

[8] Elnashar, A., & El-Saidny, M. A. (2013). Looking at LTE in practice: A performance analysis of the LTE system based on field test results. *IEEE Vehicular Technology Magazine*, *8*(3), 81-92.

[9] Simpson, O., & Sun, Y. (2018). LTE RSRP, RSRQ, RSSNR and local topography profile data for RF propagation planning and network optimization in an urban propagation environment. *Data in brief*, *21*, 1724-1737.

[10] Ramli, H. A. M., & Sukor, M. A. (2016, July). Performance analysis on automated and average channel quality information (CQI) reporting algorithm in LTE-A. In *2016 International Conference on Computer and Communication Engineering (ICCCE)* (pp. 256-260). IEEE.

[11] Kawser, M. T., Hamid, N. I. B., Hasan, M. N., Alam, M. S., & Rahman, M. M. (2012). Downlink SNR to CQI mapping for different multiple antenna techniques in LTE. *International journal of information and electronics engineering*, *2*(5), 757.

[12] Mu, Q., Liu, L., Chen, L., & Jiang, Y. (2013, October). CQI table design to support 256 QAM in small cell environment. In *2013 International Conference on Wireless Communications and Signal Processing* (pp. 1-5). IEEE.

[13] Cainey, J., Gill, B., Johnston, S., Robinson, J., & Westwood, S. (2014, September). Modeling download throughput of LTE networks. In *39th Annual IEEE Conference on Local Computer Networks Workshops* (pp. 623-628). IEEE.

[14] Sezgin, G., Coskun, Y., Basar, E., & Kurt, G. K. (2018). Performance evaluation of a live multi-site LTE network. *IEEE Access*, *6*, 49690-49704.

[15] Sevindik, V., Wang, J., Bayat, O., & Weitzen, J. (2012, October). Performance evaluation of a real long-term evolution (LTE) network. In *37th Annual IEEE Conference on Local Computer Networks-Workshops* (pp. 679-685). Ieee.

[16] Afroz, F., Subramanian, R., Heidary, R., Sandrasegaran, K., & Ahmed, S. (2015). SINR, RSRP, RSSI and RSRQ measurements in long term evolution networks. *International Journal of Wireless & Mobile Networks*.

[17] Bosneag, A. M., Handurukande, S., O'Sullivan, J., & Wang, M. (2016, April). Real-world experiences with CQI-based analyses for dense LTE networks. In *NOMS 2016-2016 IEEE/IFIP Network Operations and Management Symposium* (pp. 943-948). IEEE.

[18] Schwarz, S., Mehlführer, C., & Rupp, M. (2010, November). Low complexity approximates maximum throughput scheduling for LTE. In *2010 Conference Record of the Forty-Fourth Asilomar Conference on Signals, Systems, and Computers* (pp. 1563-1569). IEEE.

[19] Chen, X., Yi, H., Luo, H., Yu, H., & Wang, H. (2011, November). A novel CQI calculation scheme in LTE\LTE-A systems. In *2011 International Conference on Wireless Communications and Signal Processing (WCSP)* (pp. 1-5). IEEE.

[20] Akyildiz, I. F., Gutierrez-Estevez, D. M., & Reyes, E. C. (2010). The evolution to 4G cellular systems: LTE-Advanced. *Physical communication*, *3*(4), 217-244.

[21] Kim, B., & Yi, Y. (2018). *US Patent No. 9,887,824*. Washington, DC: US Patent and Trademark Office.

[22] Stojanović, I., Koprivica, M., Stojanović, N., & Nešković, A. (2020). Analysis of the impact of network architecture on signal quality in LTE technology. *Serbian Journal of Electrical Engineering*, *17*(1), 95-109.

[23] Tems investigation. (n.d.). TEMS™ Investıgatıon | Mobile Network Testing Software https://www.infovista.com/tems/investigation

[24] DeviceSpecification. (n.d.). Samsung Galaxy S6- Özellikler https://www.devicespecifications.com/tr/model/94e332dd

[25] Specht, D. F. (1991). A general regression neural network. *IEEE transactions on neural networks*, *2*(6), 568-576.

[26] Celikoglu, H. B. (2006). Application of radial basis function and generalized regression neural networks in nonlinear utility function specification for travel mode choice modeling. *Mathematical and Computer Modelling*, *44*(7-8), 640-658.

[27] Asadi, H., Shahedi, K., Jarihani, B., & Sidle, R. C. (2019). Rainfall-runoff modeling using hydrological connectivity index and artificial neural network approach. *Water*, *11*(2), 212.

[28] Yadav, A. K., Chandola, V. K., Singh, A., & Singh, B. P. (2020). Rainfall-runoff modeling using artificial neural networks (ANNs) model. *International Journal of Current Microbiology and Applied Sciences*, *9*(3), 127-135.

[29] Niwa, T. (2003). Using general regression and probabilistic neural networks to predict human intestinal absorption with topological descriptors derived from two-dimensional chemical structures. *Journal of chemical information and computer sciences*, *43*(1), 113-119.

[30] Ghritlahre, H. K., & Prasad, R. K. (2018). Exergetic performance prediction of solar air heater using MLP, GRNN and RBF models of artificial neural network technique. *Journal of environmental management*, *223*, 566-575.

[31] Izonin, I., Tkachenko, R., Verhun, V., & Zub, K. (2021). An approach towards missing data management using improved GRNN-SGTM ensemble method. *Engineering Science and Technology, an International Journal*, *24*(3), 749-759.

[32] Kurnaz, C., Engiz, B. K., & Esenalp, M. O. (2017). A novel empirical SIR-to-CQI mapping rule for DC-HSDPA systems. *Turkish Journal of Electrical Engineering & Computer Sciences*, *25*(6), 4768-4776.

[33] Kurnaz, C., Engiz, B. K., & Esenalp, M. (2017). A novel throughput mapping method for DC-HSDPA systems based on ANN. *Neural Computing and Applications*, *28*(2), 265-274.